Article

Load Estimation for Induction Heating Cookers Based on Series RLC Natural Resonant Current

Zheng-Feng Li [1,*], Jhih-Cheng Hu [1], Ming-Shi Huang [1], Yi-Liang Lin [2], Chun-Wei Lin [2] and Yu-Min Meng [2]

[1] Department of Electrical Engineering, National Taipei University of Technology (NTUT), Taipei 10608, Taiwan; t106310125@ntut.org.tw (J.-C.H.); mingshi.huang@gmail.com (M.-S.H.)
[2] Delta Electronic Inc., Taoyuan 33370, Taiwan; yiliang.lin@deltaww.com (Y.-L.L.); simon.cw.lin@deltaww.com (C.-W.L.); ian.meng@deltaww.com (Y.-M.M.)
* Correspondence: u94102@gmail.com

Abstract: In domestic induction heating applications, cookware can be considered an equivalent load in a series resistor–inductor–capacitor resonant converter. Therefore, the electrical parameters of an equivalent circuit change according to the cookware material, size and the cookware position on the heating coil. This study proposes an online estimation method for detecting the cookware status, determining the material and estimating the equivalent heating resistance of cookware on an induction heating cooker (IHC) for power control. The proposed method could turn off the circuit in abnormal situations such as low equivalent heating coverage rate or non-ferromagnetic cookware and adjust the power in normal situations. In the method, a half-bridge series resonant converter (HBSRC) generates two test patterns with three resonant voltage pulses to detect cookware every 10 ms, only the current feedback information is needed to avoid the calculation loads and times necessary for complex signal operations in software. To verify the proposed method, a digital signal processor based HBSRC with 1000 W was constructed. The maximum errors between the estimated and measured resistance and inductance were 7.14% and 2.91%, respectively. Moreover, power control in emulated user operation reveal that the proposed method and control system can effectively estimate load online to detect cookware status and determine whether to turn off or vary the heating power for an IHC.

Keywords: induction heating cooker; online load estimation; power control; series RLC resonant converter

1. Introduction

IHCs do not use an open flame, thus, they can replace gas cooktops in tall buildings and apartment complexes in earthquake-prone countries [1]. Moreover, IHCs heat both more quickly and more efficiently than conventional gas stoves do; their efficiency can exceed 80%, higher than that of gas stoves, which is only approximately 40% [2–4]. Therefore, IHCs have become popular for both domestic and commercial cooking [5,6]. In an IHC, a high-frequency magnetic flux is generated by a heating coil. This coil is driven by a half-bridge series resonant converter HBSRC as shown in Figure 1, to induce eddy currents on a thin surface of the cookware bottom, resulting in heating [7]. An HBSRC comprises a half-bridge circuit with two insulated gate bipolar transistors (IGBTs), a resonant capacitor, a heating coil, and the cookware on the heating coil. Therefore, an HBSRC can be modeled as a series resistor–inductor–capacitor (RLC) circuit, and the equivalent electrical parameters [8,9], including resistance R_{eq} and inductance L_{eq}, could be affected by the cookware material, operating frequency, and equivalent heating coverage rate (EHCR), increasing the complexity of controlling the heating power [10]. Metal cookware can be classified as ferromagnetic and non-ferromagnetic; non-ferromagnetic cookware has a small R_{eq}, resulting in a large induced current [11] and allows the control to be more difficult.

Although the R_{eq} of ferromagnetic cookware is relatively large, R_{eq} and L_{eq} can still be affected by the excitation current due to the current-dependent relative permeability of such cookware [12,13]. Moreover, the EHCR of IHC, which is determined by the geometrical alignment of the cookware and heating coil and by the bottom area of the cookware, affects R_{eq} and L_{eq}. Consequently, cookware-related parameters for an IHC cannot be obtained on a test bench in the factory; instead, R_{eq} and L_{eq} must be estimated accurately from online information about IHCs. Accordingly, modern high-end IHCs may have functions for estimating R_{eq} and L_{eq} for various pieces of cookware and their placement on the heating coil to achieve power control.
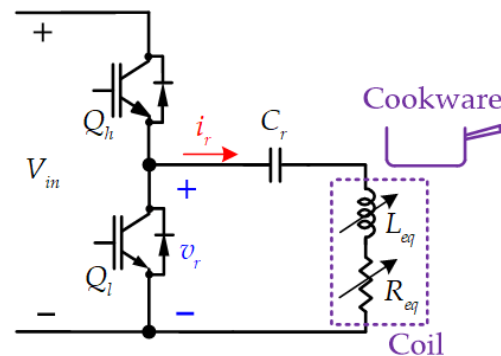

Figure 1. Equivalent circuit of an IHC.

R_{eq} and L_{eq} can be expressed in an analytical model [14–17]. One of these studies [14] proposed a mutual-inductance model of the IHC and derived R_{eq} by eddy current field. Another of these studies [15], R_{eq} and L_{eq} are calculated by eddy current loss and magnetic energy, respectively, and the impedance of IHC was obtained based on a linear interpolation between two impedances with and without considering the ferrite core of heating coil. The R_{eq} and L_{eq} were derived from the concept of electromagnetic field [16,17] and the coupling effect between coils also considered in the study [15]. Nevertheless, the correctness of derived formulas [14,16,17] was only verified by LCR meter without considering magnetic saturation on the ferromagnetic cookware. Studies and comparison on the load estimation methods of the IHC are shown in Table 1. R_{eq} and L_{eq} can be estimated either offline or online. In offline calculation methods, R_{eq} and L_{eq} can be calculated according to the fundamental frequency impedance [18] or resonant capacitor voltage and quality factor [19]. Several studies have focused on developing online estimation methods for reducing the effects of variations in R_{eq} and L_{eq} on power control due to cookware movement or removal from the heating coil during heating. For example, studies [20–22] have proposed online estimation methods for quasi-resonant converters. Specifically, one of these studies [20] proposed four estimation methods for measuring the V_{CE} of an IGBT under constant current control, measuring the turn-on current I_C of the IGBT under constant voltage control, comparing times at which V_{CE} is greater than the DC link voltage, and measuring the diode turn-on time. Another of these studies [21] used the voltage, current waveform, and related period under different switching intervals to calculate equivalent parameters. [22] detected equivalent parameters by using the power factor and the absolute amplitude of the impedance |Z|. As IHCs based on quasi-resonant converters have the shortage of high-voltage stress on the power transistors [23], many studies [24–30] have focused on estimation methods for HBSRCs; specifically, these studies have proposed estimation methods based on single values or the average value of feedback electrical signals within a bus voltage cycle [24–27]. One of these studies [24] used a phase-sensitive detector, the inputs of which are multiplied by sine and cosine signals of the feedback voltage and current, respectively, and calculated R_{eq} and L_{eq} by using a low-pass filter. Another of these studies [25] adopted a first-order delta–sigma algorithm to digitize the feedback signals of the resonant voltage and current and then used the discrete Fourier transform (DFT) to calculate R_{eq} and L_{eq}. In addition, another of these studies [26] adopted particle

swarm optimization to obtain the average equivalent resistance. Finally, [27] measured the resonant capacitor voltage and voltage harmonics for estimation. A study also determined the EHCR of cookware by using deep learning [28]. Two studies [29,30] have considered the influence of bus voltage variations on R_{eq} and L_{eq} estimations. Furthermore, another study [31] executed power control by changing the operating frequency; the study used the DFT to calculate the equivalent impedance from the resonant voltage and current in an area with a relatively high DC-link voltage in order to achieve favorable power control. Most of the aforementioned online estimation methods require first collecting substantial voltage and current data and then using a field-programmable gate array to perform complex calculations. The calculation capacity of cost-effective microprocessors is limited. Accordingly, this study proposes a method that requires sampling only several specified current values at periodic times during the natural resonant period to perform online R_{eq}, and L_{eq} estimation for cookware in order to execute power control.

Table 1. Studies and comparison on the load estimation methods of the IHC. Note: Half bridge (HB), quasi-resonant (QR).

Refs.	Estimation Method of Load Impedance	Feedback	Circuit Topology	Online Estimation	Computation Loading	Accuracy
[18]	Discrete-Time Fourier Series coefficients from voltage and current waveform.	Voltage and current	HB	×	High	High
[19]	Resonant voltage and quality factor (Q).	Voltage	HB	×	High	High
[20]	1. V_{CE} under constant current control. 2. I_C under constant voltage control. 3. comparing times at which V_{CE} is greater than the DC link voltage. 4. measuring the diode turn-on time.	Voltage or current	QR	○	low	N/A
[21]	Voltage, current waveform, and related period under different switching intervals	Voltage and current	QR	○	Middle	Low
[22]	Power factor and the absolute amplitude of the impedance.	Voltage and current	QR	○	Low	Middle
[24]	A phase-sensitive detector (PSD) is used to decouple the feedback voltage and current.	Voltage and current	HB	○	High	High
[25]	Using first-order delta–sigma algorithm to digitize the feedback signals of the resonant voltage and current and then calculated the load impedance by discrete Fourier transform.	Voltage and current	HB	○	Middle	Middle
[26]	Particle swarm optimization.	Voltage and current	HB	○	High	High
[27]	Measured the resonant capacitor voltage and voltage harmonics.	Voltage and current	HB	○	Middle	High
[28]	Deep learning from experimental data.	Power, current and Q	HB	○	High	High
[29]	Similar to [24].	Voltage and current	HB	○	High	High
[30]	Combination with PSD and deep learning.	Voltage and current	HB	○	High	High
Proposed method	Key points of current in natural resonant period.	Current	HB	○	Low	High

This paper presents a digital signal processor (DSP)-based digitally controlled IHC system with the proposed online load estimation method for detecting whether the cookware has normal or abnormal status and for measuring the R_{eq} to achieve continuous power control. Moreover, the proposed online load estimation method requires only information about the resonant current i_r, namely the current at the high-side IGBT turn-off transient,

the time of the first negative half-cycle, and the peak current during the natural resonant period in an HBSRC, only the resonant current information is needed for the proposed method to reduce the calculation loads and times for complex signal operations in software and achieve accurate estimation results. This study derived formulas for the estimated equivalent resistance R_{est} and equivalent inductance L_{eq} and verified them by using the simulation software Simulink. To verify the proposed online load estimation method, a measurement method based on two fundamental components, namely the resonant voltage v_r and resonant current i_r, was used to calculate R_{eq} and L_{eq} for comparison. The fundamental frequency components v_r and i_r were obtained using bandpass filters in a dual-channel programmable filter equipment (NF 3627) to reach high accuracy. Through the proposed method, R_{est} and the amplitude of i_r were estimated as power feedback in a closed loop for power control. R_{eq} and L_{eq} estimation for normal cookware including that for abnormal cookware detection, and power control were proposed to achieve more accurate heating power control through online load estimation for IHCs. Finally, to verify the proposed online load estimation method, a DSP-based IHC with a rated power of 1000 W was constructed with the specification shown in Table 2 and examined using both ferromagnetic and non-ferromagnetic cookware at different EHCRs. The maximum error between the estimated R_{est} and measured R_{eq} was only 3.55% for ferromagnetic cookware, and the experimental results regarding power control indicated that the proposed method can effectively estimate both R_{eq} and L_{eq} online to detect cookware status on an IHC and control heating power.

Table 2. Electrical specifications of the proposed IHC.

Parameter	Value
Rated input DC voltage (V)	150
Rated output power (W)	1000
Switching frequency f_s (kHz)	20
Resonant capacitor (nF)	970
Intermittent estimation period (ms)	10

2. Characteristics of Cookware on an IHC

As cookware materials are excessively complex for modeling or analysis with simulation software, study [32] proposed the impedance measured method by the voltage and current waveforms across the inductor which consists of R_{eq} and L_{eq}. However, when the R_{eq} is much smaller than the reactance of L_{eq}, the phase between measured voltage and current is closed to 90° to increase the measured errors of R_{eq}. This study proposes a measurement method for L_{eq} and R_{eq} of cookware on an IHC shown in Figure 2. The proposed method uses the fundamental frequency components of resonant voltage v_r and current i_r to calculate L_{eq} and R_{eq}; the L_{eq} and R_{eq} formulas can be expressed as follows:

$$L_{eq} = \frac{\frac{V_{rp1}}{I_{rp1}} \sin(\theta_{v1} - \theta_{i1}) + \frac{1}{2\pi f_s C_r}}{2\pi f_s} \tag{1}$$

$$R_{eq} = \frac{V_{rp1}}{I_{rp1}} \cos(\theta_{v1} - \theta_{i1}) \tag{2}$$

$$v_{r1}(t) = V_{rp1} \sin(2\pi f_s t + \theta_{v1}) \tag{3}$$

$$i_{r1}(t) = I_{rp1} \sin(2\pi f_s t + \theta_{i1}) \tag{4}$$

where the variables are defined as follows:

v_{r1} and i_{r1}: resonant voltage v_r and current i_r, respectively, representing the fundamental frequency components.
V_{rp1} and I_{rp1}: amplitude of v_{r1} and i_{r1}, respectively.
θ_{v1} and θ_{i1}: phase angle of v_{r1} and i_{r1}, respectively.

(**a**)   (**b**)
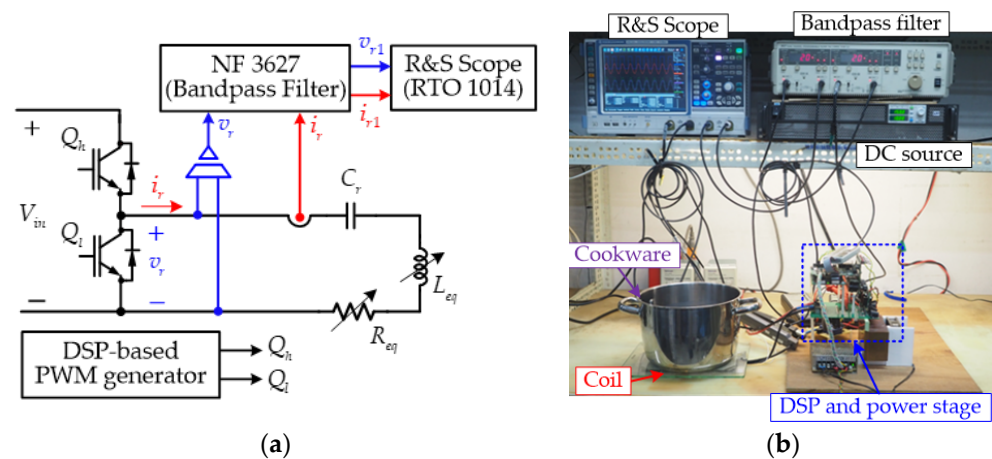
Figure 2. Proposed R_{eq} and L_{eq} measurement method: (**a**) Test function block; (**b**) Test setup.

To measure v_{r1} and i_{r1}, this study used bandpass filters with a center frequency at f_s in an NF 3627 system, and the HBSRC was operated at f_s with a 50% duty cycle. As shown in Table 3, two types of cookware (ferromagnetic and non-ferromagnetic) were used for testing and to calculate R_{eq} and L_{eq} at different operating currents, frequencies, and EHCRs. Figure 3 shows the EHCR as defined in the test. The influence of operating current, frequency, and EHCR on R_{eq} and L_{eq} could thus be measured. Moreover, the measured R_{eq} and L_{eq} values of the heating coil without cookware were 0.15 Ω and 77.9 μH, respectively.

Table 3. Tested cookware.

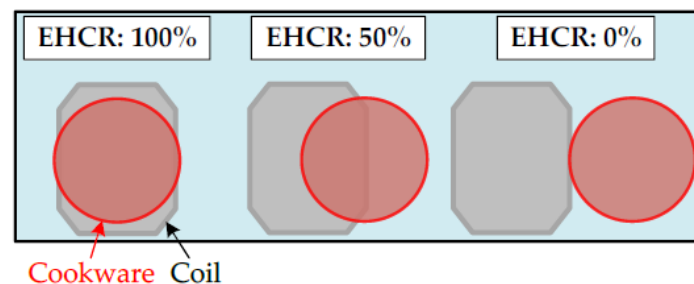| Cookware Type	A	B
Photo		
Bottom side diameter	180 mm	180 mm
Material	Ferromagnetic	Non-ferromagnetic (copper)

Figure 3. EHCR as defined in the tests.

2.1. Measurement at Different Operating Currents

Figure 4 shows the test results obtained by varying the peak current I_{rp1} from 1 to 25 A by adjusting V_{in} at a fixed f_s value of 20 kHz and 100% EHCR. Non-ferromagnetic cookware does not have hysteresis losses and have a relative permeability level of approximately 1. Accordingly, the R_{eq} and L_{eq} values of the non-ferromagnetic cookware were not affected by the applied I_{rp1}, and the measured R_{eq} values were considerably smaller than the ferromagnetic cookware.
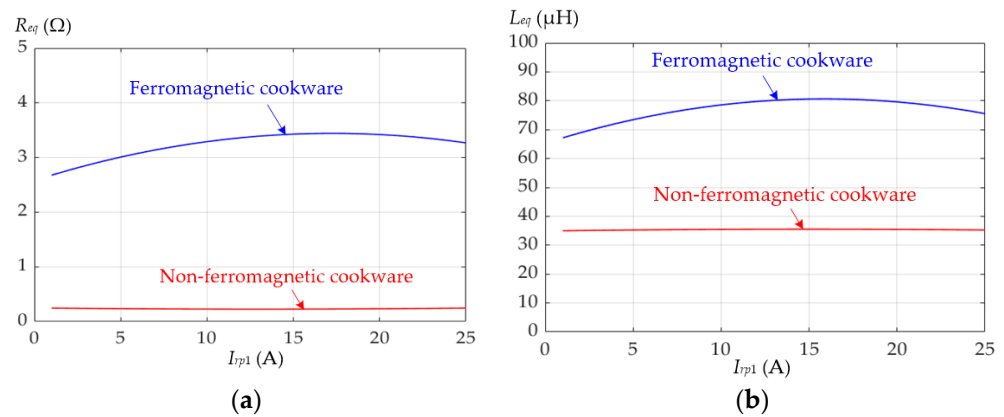
Figure 4. Measured R_{eq} and L_{eq} of the ferromagnetic and non-ferromagnetic cookware at different I_{rp1}: (**a**) R_{eq}; (**b**) L_{eq}. ($f_s = 20$ kHz, EHCR $= 100\%$).

2.2. Measurement at Different Operating Frequencies

R_{eq} and L_{eq} were also measured at operating frequencies f_s ranging from 15 to 30 kHz at an I_{rp1} value of 20 A and 100% EHCR; the results are shown in Figure 5. Ferromagnetic cookware has a higher coupling magnetic flux than non-ferromagnetic cookware does. Hence, the R_{eq} values of the ferromagnetic cookware clearly increased with the operating frequency. However, the magnetic flux caused by increasing eddy currents at the bottom of the ferromagnetic cookware counteracted the magnetic flux generated by the heating coil, possibly reducing L_{eq}.
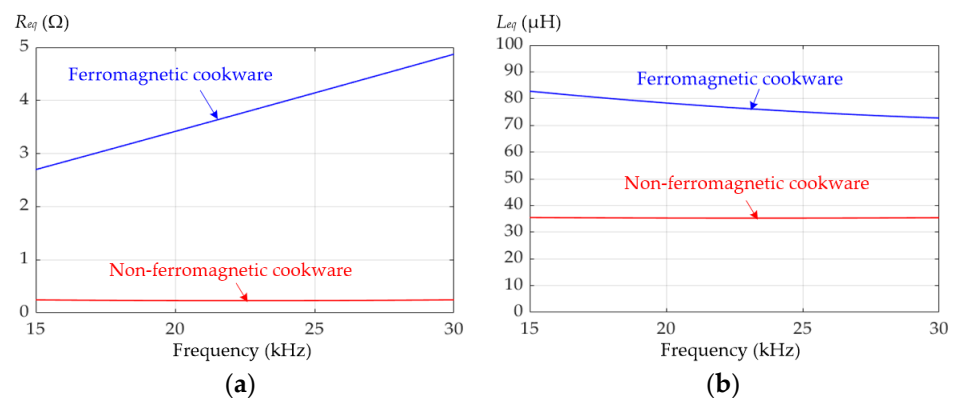

Figure 5. Measured R_{eq} and L_{eq} of ferromagnetic and non-ferromagnetic cookware at different operating frequency: (**a**) R_{eq}; (**b**) L_{eq}. (EHCR $= 100\%$, $I_{rp1} = 20$ A).

2.3. Measurement at Different EHCRs

R_{eq} and L_{eq} were measured at EHCRs ranging from 0% to 100% at an I_{rp1} value of 20 A and f_s of 20 kHz, and the results are shown in Figure 6. The results revealed that the eddy currents and hysteresis losses in the ferromagnetic cookware clearly increased with the EHCR. Although the coupling magnetic flux may increase with the EHCR, the relative permeability of the ferromagnetic cookware was reduced due to magnetic flux saturation at high EHCRs. Thus, variations in L_{eq} were comparatively subtle. By contrast, the relative permeability of the non-ferromagnetic cookware was near unity; thus, L_{eq} decreased as the EHCR increased. Moreover, the load characteristic of non-metal and non-ferromagnetic cookware (e.g., glass) is similar to no load (EHCR = 0%).
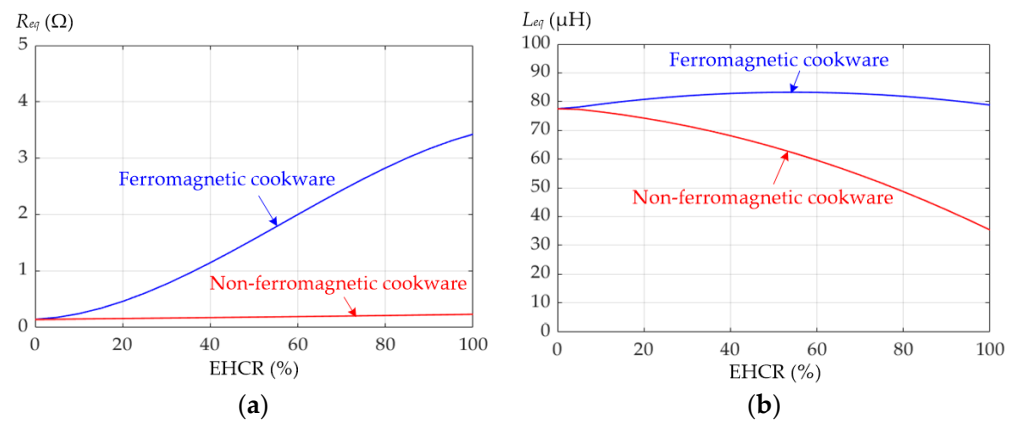
Figure 6. Measured R_{eq} and L_{eq} of ferromagnetic and non-ferromagnetic cookware at different EHCRs: (**a**) R_{eq}; (**b**) L_{eq}. ($f_s = 20$ kHz, $I_{rp1} = 20$ A).

On the basis of the R_{eq} and L_{eq} values measured for the ferromagnetic and non-ferromagnetic cookware by using the proposed method, the following conclusions could be drawn:

1. The non-ferromagnetic cookware had substantially lower R_{eq} and L_{eq} values; thus, these results can be used as an index to determine the cookware material. As this study focused on R_{eq} and L_{eq} estimation for ferromagnetic cookware, the HBSRC can be turned off if the cookware is non-ferromagnetic;
2. For the ferromagnetic cookware, L_{eq} variations were small as I_{rp1}, operating frequency, and EHCR increased;
3. The R_{eq} values measured for the ferromagnetic cookware changed substantially as the EHCR increased. Therefore, R_{eq} can be used to detect when the ferromagnetic cookware is moved during heating. For an IHC, I_{rp1} can be adjusted to maintain constant power or to turn off the power when the EHCR is low. The IHC used in this study turned off the power when the EHCR was less than 50%.

3. Proposed Load Estimation Method and Power Control System

Figure 7 shows the equivalent circuits of an HBSRC in different operating periods, and Figure 8 displays the waveforms of the resonant voltage v_r and current i_r of a series RLC circuit. The circuit operation is outlined as follows: First, the DC link voltage V_{in} is sent to the series RLC circuit when the IGBTs Q_h and Q_l are in on and off states, respectively. Subsequently, the IGBTs Q_h and Q_l enter the off and on states, respectively, and the series RLC circuit is operated at its natural resonant period.
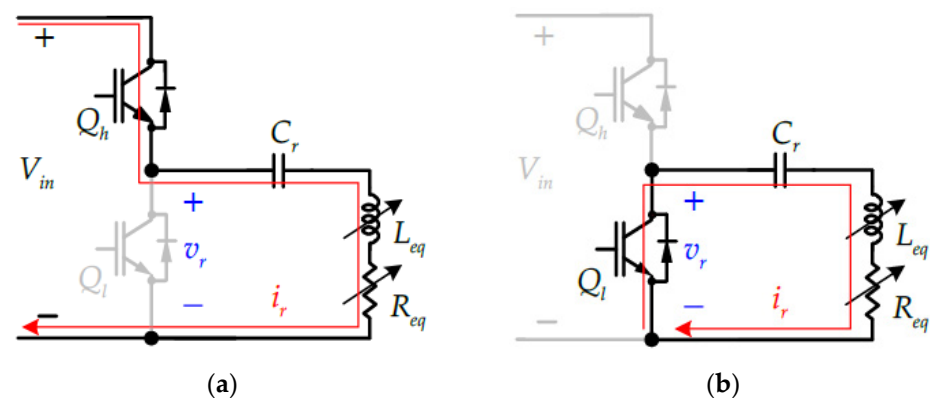

Figure 7. Equivalent circuit of an HBSRC in different operating intervals: (**a**) line power transmission interval; (**b**) natural resonant period.
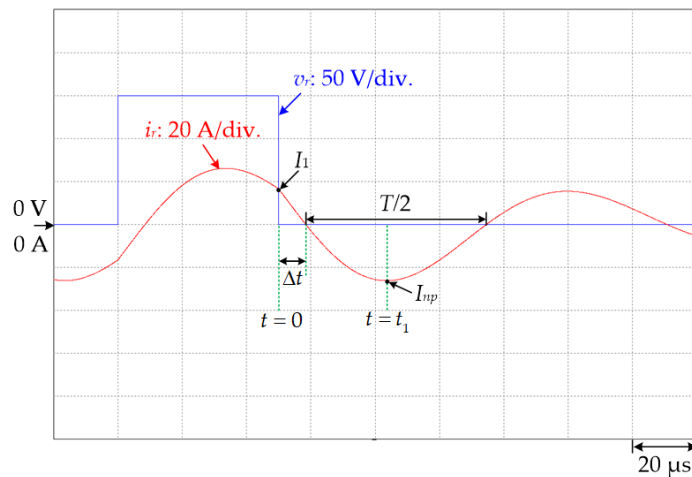
Figure 8. Waveform of v_r and i_r in the HBSRC.

3.1. Estimation Method for Equivalent Impedance

If the dead-time effect is neglected, the resonant current i_r during the natural resonant period can be derived as follows [20,21,33–35]:

$$i_r(t) = e^{-\alpha t}[B_1 \cos \omega_d t + B_2 \sin \omega_d t] \tag{5}$$

The initial conditions of $i_r(0)$ and its derivative $\frac{d}{dt}i_r(0)$ during natural resonant period can be expressed as follows:

$$i_r(0) = I_1 \,, \quad \frac{di_r(0)}{dt} = \frac{-1}{L_{est}}(R_{est}I_1 + V_{C0}) \tag{6}$$

wherein,

$\omega_d(= \sqrt{\omega_o{}^2 - \alpha^2})$: damping resonant angular frequency.

$\omega_o(= \frac{1}{\sqrt{L_{est}C_r}})$: natural resonant angular frequency.

$\alpha(= \frac{R_{est}}{2L_{est}})$: damping coefficient.

B_1, B_2: coefficients;

C_r: resonant capacitor;

L_{est}: estimated equivalent inductance;

R_{est}: estimated equivalent resistance;

V_{C0}: initial value of resonant capacitor voltage at the beginning of natural resonant period;

I_1: initial value of the resonant current i_r at the beginning of natural resonant period.

Substituting Equation (6) into Equation (5) yields the following:

$$i_r(t) = e^{-\alpha t}[I_1 \cos \omega_d t - \frac{R_{est}I_1 + 2V_{c0}}{2L_{est}\omega_d} \sin \omega_d t] \tag{7}$$

As $\omega_o{}^2$ is much larger than α^2 in IHC applications, ω_d can be replaced by ω_o. Therefore, Equation (7) can be simplified and expressed as follows:

$$i_r(t) = I_P e^{-\alpha t} \sin(\omega_o t + \theta) \tag{8}$$

where

$$I_p = \sqrt{I_1{}^2 + (\frac{R_{est}I_1 + 2V_{C0}}{2L_{est}\omega_o})^2} \tag{9}$$

$$\theta = \tan^{-1}(\frac{2L_{est}\omega_o I_1}{R_{est}I_1 + 2V_{C0}}) \tag{10}$$

If the negative half-period time is $T/2$ and the first zero-crossing time Δt, I_1 and the peak resonant current in the negative period I_{np} can be measured, R_{est} and L_{est} can be derived as follows:

$$R_{est} = \frac{2L_{est}}{\Delta t + \frac{T}{4}} \ln\left(\frac{-I_1}{I_{np}} \frac{1}{\sin(2\pi\frac{\Delta t}{T})}\right) \tag{11}$$

$$L_{est} = \left(\frac{1}{2\pi f_o \sqrt{C_r}}\right)^2 \tag{12}$$

3.2. Simulation Results of the Proposed Estimation Method

To verify the effectiveness of the proposed load estimation method, several simulations of cookware on a heating coil were performed under four operating, which involved varying operating frequencies, duty cycles, equivalent impedances, and equivalent resistances. $T/2$, Δt, I_1 and I_{np} could be measured from the simulated waveforms shown in Figure 9, and R_{est} and L_{est} could be derived using Equations (11) and (12). The estimation results derived under the four conditions are listed in Table 4. The maximum errors between the estimated and preset inductances (error of inductance, EOI) and resistances (error of resistance, EOR) were 2.4% and 3.3%, respectively, indicating the effectiveness of the proposed load estimation method.
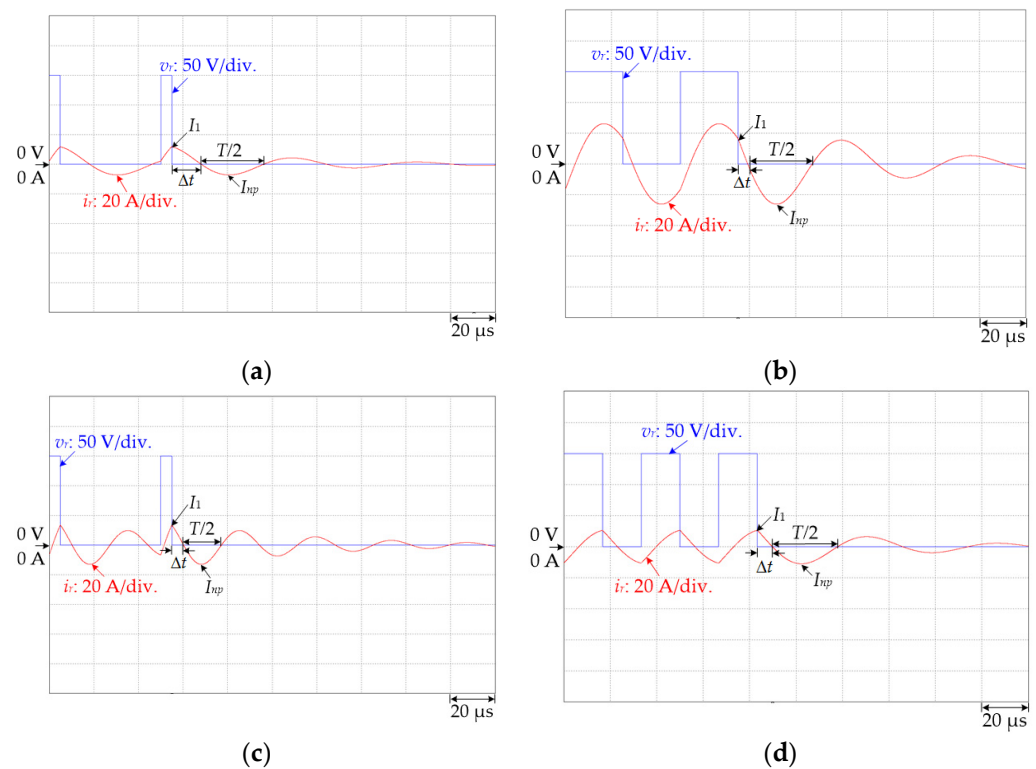

Figure 9. Simulated resonant waveforms of v_r and i_r: (**a**) condition 1; (**b**) condition 2; (**c**) condition 3; (**d**) condition 4.

Table 4. Simulated results of the estimated impedance derived under different conditions.

	Condition	1	2	3	4
Preset values	DC link voltage V_{in} (V)		150		
	Frequency (kHz)	20	20	20	40
	Duty (%)	10	50	10	50
	L_{eq} (μH)	80	80	30	80
	R_{eq} (Ω)	3	3	1	3
Simulated results	I_1 (A)	11.8	16.1	13.3	10.5
	I_{np} (A)	−7.3	−26.1	−13.0	−11.0
	Δt (μs)	18	4.1	5.2	6.5
	$T/2$ (μs)	28.0	28.0	17.0	28.0
Estimated results	L_{est} (μH)	81.9	81.9	30.2	81.9
	R_{est} (Ω)	3.0	3.0	1.0	2.9
Error	Equivalent inductance EOI (%)	2.4	2.4	0.7	2.4
	Equivalent resistance EOR (%)	0.0	0.0	0.0	3.3

where, EOI (%) $= \left| \frac{L_{est} - L_{eq}}{L_{eq}} \right| \times 100\%$, EOR (%) $= \left| \frac{R_{est} - R_{eq}}{R_{eq}} \right| \times 100\%$

3.3. Cookware Estimation and Power Control Procedure

The proposed control system, comprising a power control module and a load estimation module, is shown in Figure 10. The HBSRC generates two test patterns with three resonant voltage pulses to detect cookware every 10 ms; each cycle includes a 1 ms estimation time and 9 ms power control time. The power control module uses the fundamental frequency power P_1, which can be expressed as follows:

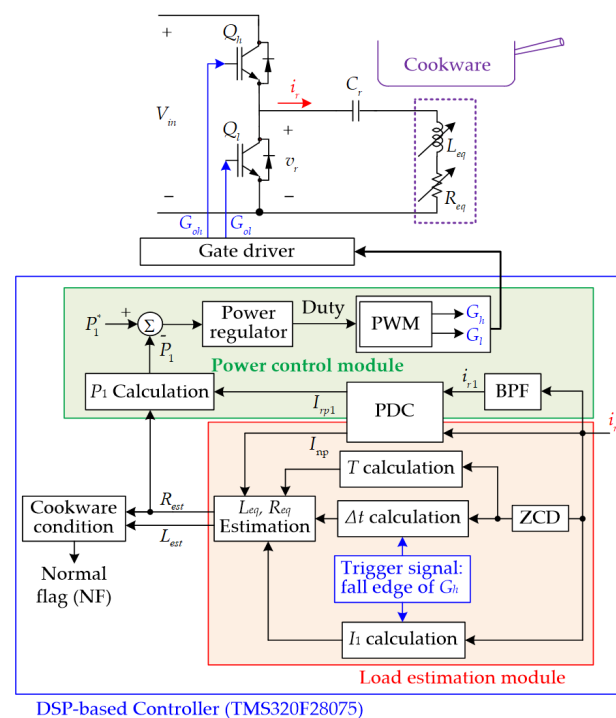$$P_1 = \frac{1}{2} I_{rp1}^2 R_{est} \tag{13}$$

Figure 10. Proposed control methodology. (note: * is defined as command.)

I_{rp1} is generated by passing the i_r through a bandpass filter at a center frequency of f_s and is measured with a peak detector circuit (PDC). R_{est} is obtained using Equation (11).

The power regulator comprises a PI-type regulator, which generates a duty command for the HBSRC with fixed f_s to achieve the required heating power.

To estimate R_{eq} and L_{eq} in this study, hardware circuits for the bandpass filter, PDC, and zero cross detector (ZCD) were adopted to avoid the calculation loads and times necessary for complex signal operations in software. Thus, the necessary signals for the proposed estimation method in Equations (11) and (12) could be easily obtained. Some details of the proposed load estimation module are presented as follows:

1. I_{np} can be obtained from the negative peak value of i_r by using the PDC;
2. $T/2$ can be obtained using an embedded high-speed counter, and the capture function of the DSP can be used to calculate the time at which two adjacent zero-crossing signals of i_r are output by the ZCD;
3. Δt can be calculated using the time difference between the falling edge signal G_h and the first signal generated by the ZCD when the first zero-crossing signal of i_r is detected during the natural resonant period. Moreover, the time difference can be obtained using the same mechanism as for $T/2$;
4. I_1 can be captured using the embedded analog-to-digital converter in the DSP; the converter is triggered by the falling edge signal G_h;
5. If R_{est} and L_{est} indicate that the cookware is both ferromagnetic and on the heating coil, the cookware is heated. Otherwise, the HBSRC is turned off.

Figure 11 shows a flowchart of the proposed control system, which is synchronous with the operating frequency (20 kHz). That is, an interrupt (INT) is generated at each 50 µs period to trigger R_{est} and L_{est} estimation and power control. The two flags ENest and ENpower in the control flowchart indicate these operations, and the functions of the key blocks are as follows:

1. The variable N is a counter of the INTs to generate a period of 10 ms for R_{est} and L_{est} estimation;
2. An ENest value of 1 indicates live execution of R_{est} and L_{est} estimation;
3. An ENest value of 0 and ENpower value of 0 indicate that the cookware is non-ferromagnetic or is not on the heating coil, prompting the heating power to be turned off;
4. An ENest value of 0 and ENpower value of 1 indicates that the ferromagnetic cookware is being heated under constant power control using R_{est}.
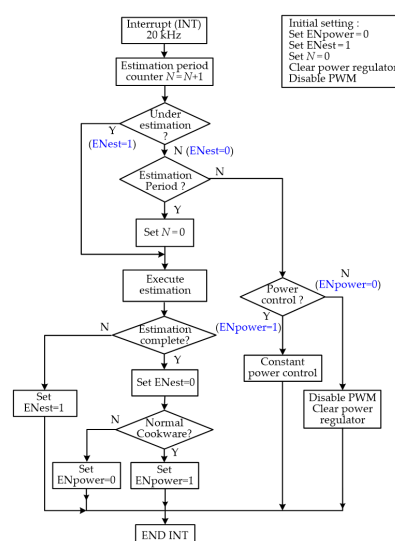

Figure 11. Flowchart of proposed control system for an IHC.

To demonstrate an example of the control system, Figure 12 shows a control pattern for v_r under normal and abnormal conditions. In this example, three continuous v_r pulses,

with 10% duty and spaced at 50 μs, are first adopted to determine whether the cookware status is normal or abnormal. The duty is set to 10% to prevent the non-ferromagnetic cookware or low EHCR from inducing a larger resonant current that may destroy IGBTs. If the cookware status is determined be normal, three continuous v_r pulses, with 50% duty spaced at 50 μs, are used to derive L_{est} and R_{est}. Finally, the heating power control system is implemented according to the heating power, as indicated in Equation (13). The control process for normal cookware is presented in Figure 12a. If the cookware status is determined be abnormal, the heating power control is turned off, as shown in Figure 12b.
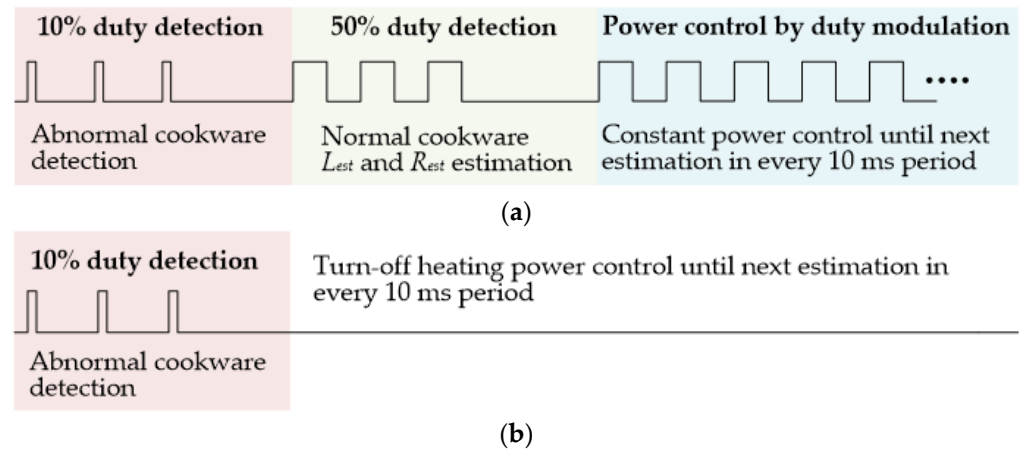

(a)

(b)

Figure 12. Proposed control pattern of v_r under two conditions: (**a**) normal; (**b**) abnormal.

4. Experimental Results

The test setup and platform comprised an HBSRC, cookware, a digital scope (R&S RTO1014, Munich, Germany), a recorder (Yokogawa DL850, Tokyo, Japan), and the proposed DSP-based IHC, as shown in Figure 13. The proposed load measurement method shown in Figure 2 was verified by implementing it to measure R_{eq} and L_{eq} simultaneously.
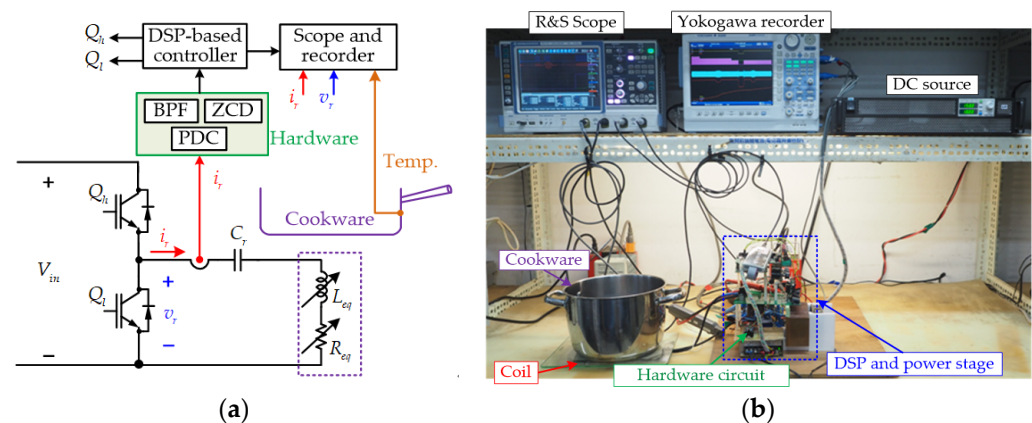

(a)

(b)

Figure 13. Test setup for verifying the proposed R_{eq} and L_{eq} estimation method and power control system for the implemented IHC system: (**a**) test function block and (**b**) test platform.

4.1. R_{eq} and L_{eq} Verification

Several test conditions shown in Table 5 including different EHCRs and cookware materials for various cases were used to verify the effectiveness of the proposed load estimation method. Cases 3 and 4 represented an abnormal condition under which the controller should turn off the heating power. As a low R_{eq} of the heating coil due to the absence of cookware or non-ferromagnetic cookware may induce a large resonant current i_r, the test duty for Cases 3 and 4 was limited to 10% to prevent a large i_r from damaging the HBSRC IGBTs.

Table 5. Test conditions involving different EHCR and cookware materials for various cases.

Test Conditions	Normal Situation		Abnormal Situation	
	Case 1	Case 2	Case 3	Case 4
Cookware material	Ferromagnetic	Ferromagnetic	Without cookware	Non-ferromagnetic
Frequency (kHz)	20	20	20	20
EHCR (%)	100	50	0	100
Duty (%)	50	50	10	10

Figure 14 presents the v_{r1} and i_{r1} results generated by passing v_r and i_r through the NF 3627 bandpass filter shown in Figure 2; the generated results were sufficient for calculating L_{eq} and R_{eq} using Equations (1) and (2), respectively.
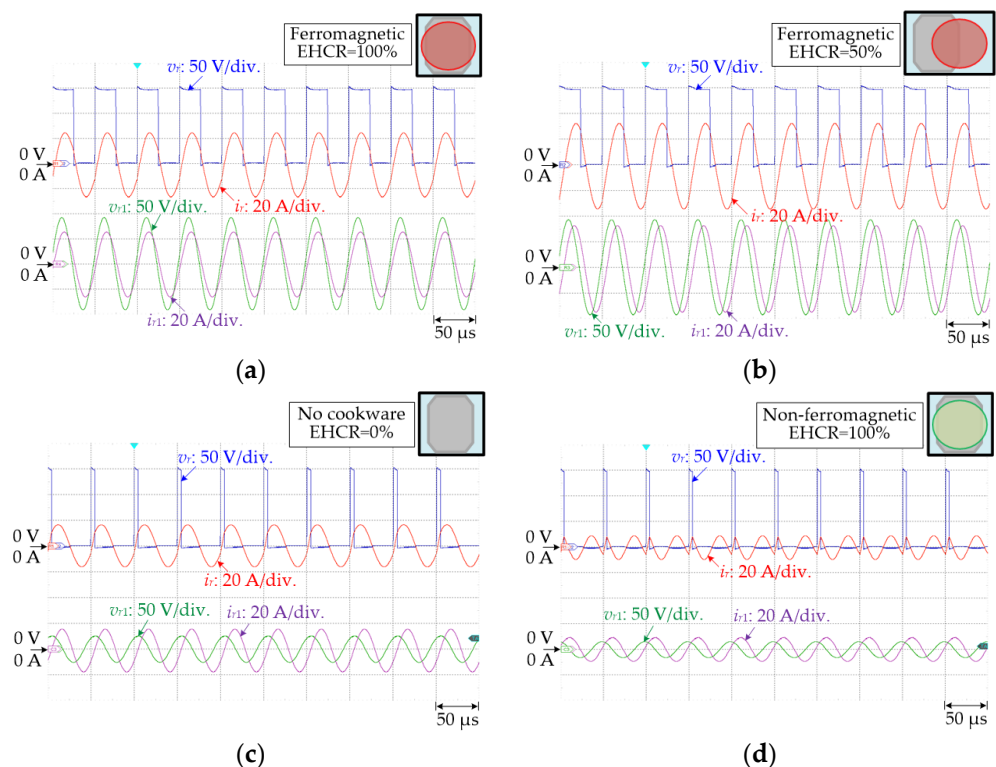

Figure 14. Measured results for test conditions: (**a**) Case 1; (**b**) Case 2; (**c**) Case 3 (**d**) Case 4.

Figure 15 presents the load estimation results; R_{est} and L_{est} were calculated online through Equations (11) and (12) by using values obtained from the digital-to-analog converter in the DSP-based controller. If the proposed estimation method detects that L_{est} is excessively small, it assumes that the cookware is non-ferromagnetic and does not calculate R_{est} shown in Figure 15d. The measurement and online estimation results for load impedance are summarized in Table 6. The maximum errors between the measured and estimated inductance and resistance values for the normal situation were 2.91% and 3.55%, respectively, signifying the effectiveness of the proposed load estimation method. Moreover, the required time for online calculations was less than 100 μs after the falling edge of the last tested pulse-width modulation cycle.
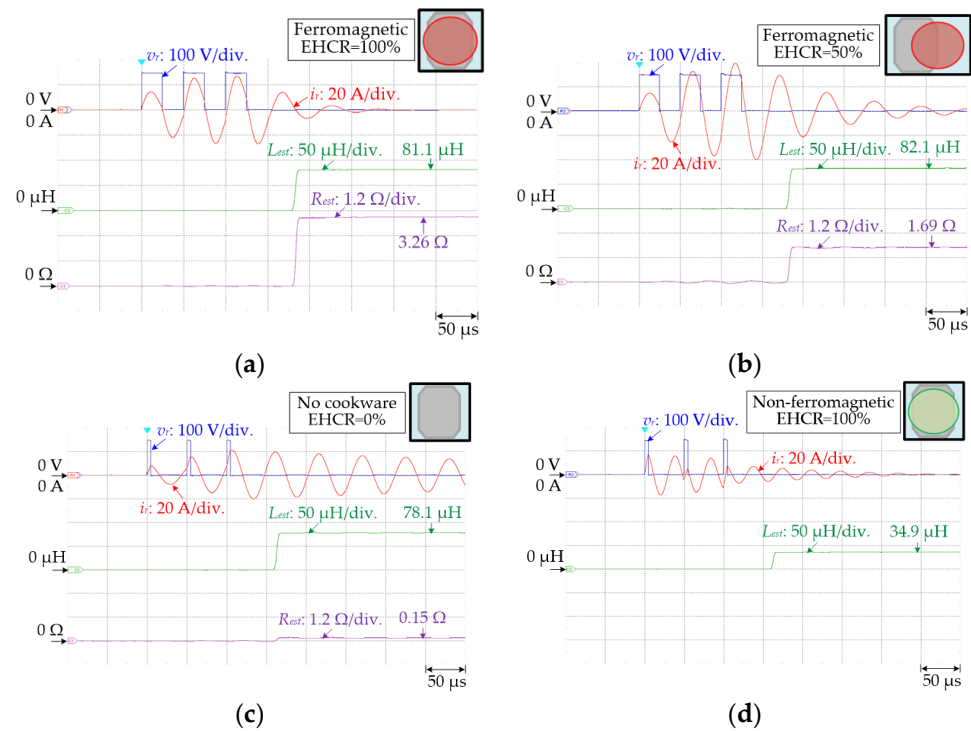
Figure 15. Experimental result for the proposed estimation method: (**a**) Case 1; (**b**) Case 2; (**c**) Case 3; (**d**) Case 4.

Table 6. Measured and estimated results for the test cases in Table 5.

Experimental Method	Experimental Results	Normal Situation		Abnormal Situation	
		Case 1	Case 2	Case 3	Case 4
Measurement	L_{eq} (μH)	78.8	83.4	77.9	35.9
	R_{eq} (Ω)	3.38	1.66	0.14	0.23
Estimation	L_{est} (μH)	81.1	82.1	78.1	34.9
	R_{est} (Ω)	3.26	1.69	0.15	N/A
Error	EOI (%)	2.91	1.56	0.26	2.78
	EOR (%)	3.55	1.81	7.14	N/A

4.2. Varying EHCRs during Heating

To test the ability of the proposed method to detect whether the ferromagnetic cookware is placed on the IHC, the tested cookware was moved to the center of the heating coil and then gradually moved away to change the EHCR during the test. As shown in Figure 16, the calculated R_{est} and L_{est} changed in accordance with the cookware position. NF was set to 1 if R_{est} was higher than 1.7 Ω, indicating that the EHCR was nearly 50% and the cookware was ferromagnetic.
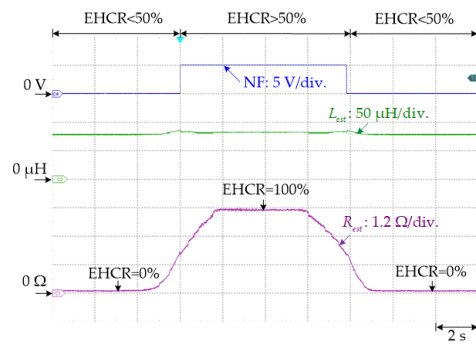
Figure 16. Experimental results for the proposed estimation method with different EHCR.

4.3. Estimation Pattern in Abnormal and Normal Situation

Figure 17 shows the controlled resonant voltage and current for different cookware situations, including non-ferromagnetic cookware, ferromagnetic cookware with an EHCR of 0%, and ferromagnetic cookware with an EHCR of 100%. On the basis of the calculations (conducted at 10 ms intervals) of the proposed method, heating occurred in only the normal situation that involved ferromagnetic cookware with an EHCR of 100%.
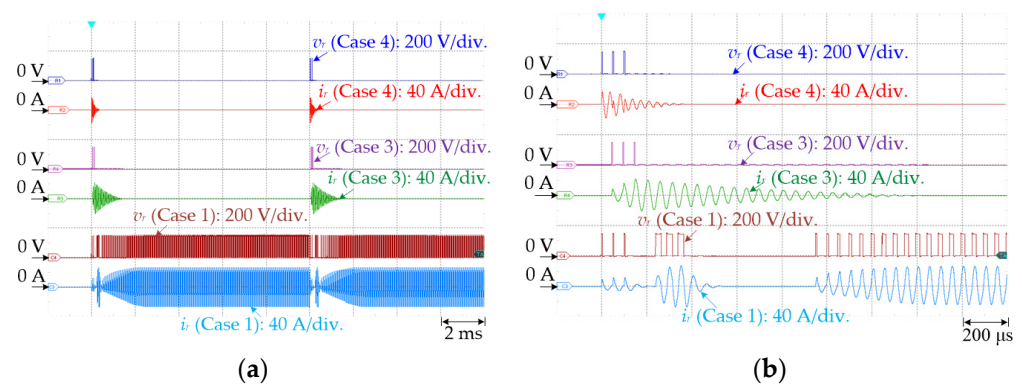

Figure 17. Experimental results for the controlled resonant voltage and current for different cookware situations: (**a**) Full estimation and power control; (**b**) zoomed-in waveform during the estimation period.

4.4. Constant Power Control

Figures 18 and 19 illustrate the experimental results for power control at 500 and 1000 W, respectively. The step response time of the power control system was less than 2 ms, and the steady-state command tracking error was approximately 0, indicating that the proposed load estimation method and power control system exhibited excellent performance.
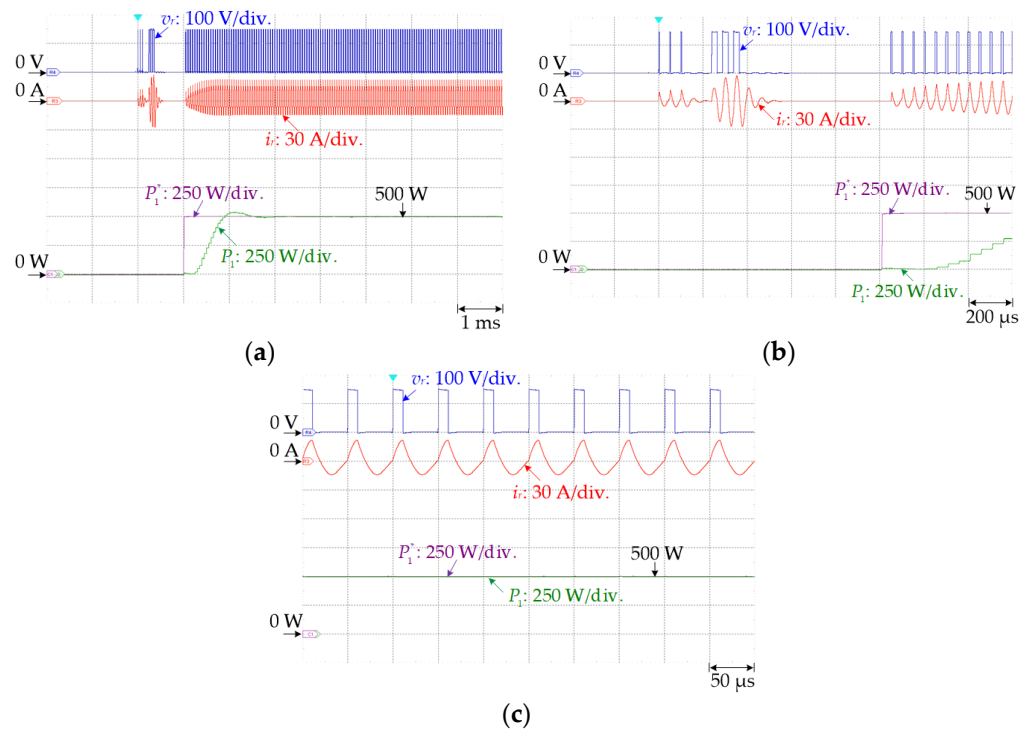
Figure 18. Experimental results for power control under 50% rated load (500 W): (**a**) full estimation and power control; (**b**) zoomed-in waveform for estimation; (**c**) zoomed-in waveform for power control. (note: * is defined as command.)

Figure 19. Experimental results for power control under 100% rated load (1000 W): (**a**) full estimation and power control; (**b**) zoomed-in waveform for estimation; (**c**) zoomed-in waveform for power control. (note: * is defined as command.)
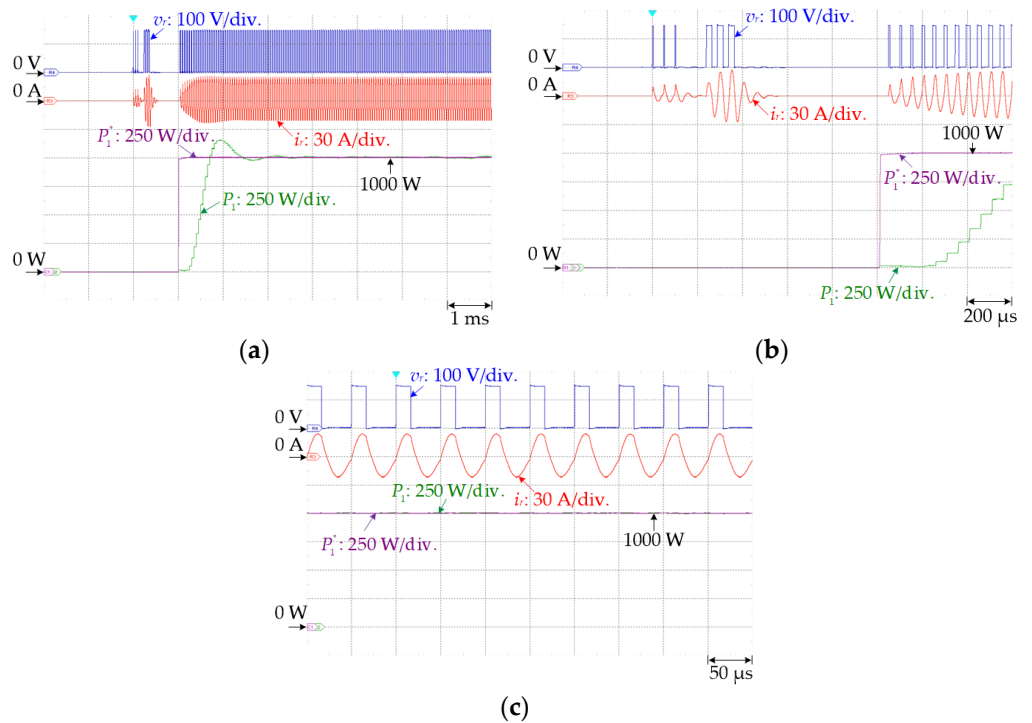
Figure 20 shows the experimental results for power control for emulated user operation. The starting power was set to 1000 W (i.e., 100% rated output), followed by 750 and

500 W in succession. The following performance results were obtained for the proposed control system:

1. Favorable constant power control was achieved by adjusting the duty value despite the EHCR changing between 100% and 70%. In Figure 20, the green block represents the waveform for P_1 derived after R_{est} estimations at 10 ms intervals. The peak envelope power P_1 was close to the desired power P_1^*;

2. According to the NF signal, the power was turned off or on when R_{est} was lower or higher, respectively, than 1.7 Ω.
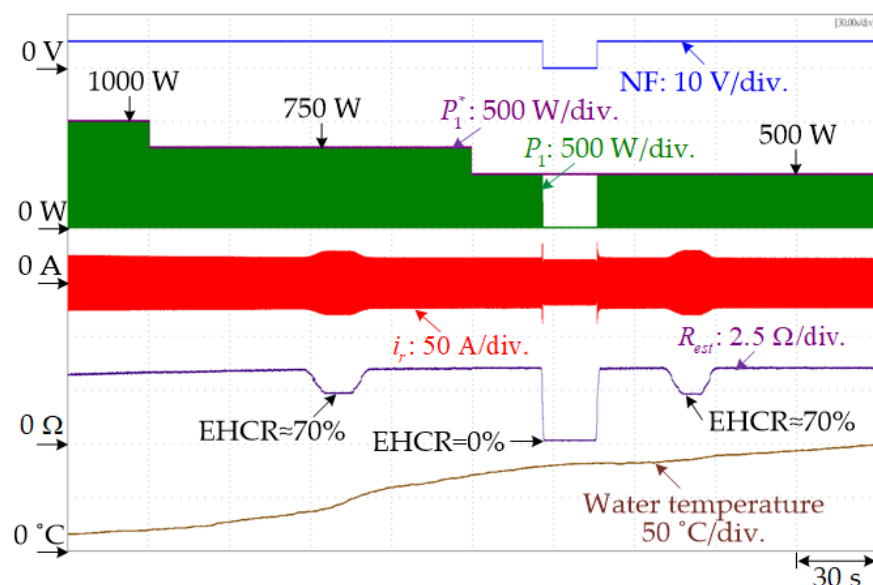

Figure 20. Power control system results for an IHC under emulated user operation. (note: * is defined as command.)

5. Conclusions

This study proposes a DSP-based digitally controlled IHC system with an online load estimation method for detecting normal or abnormal cookware status and for obtaining the equivalent heating resistance R_{eq} to achieve constant power control. The online load estimation method requires only an i_r feedback signal and simple calculations; the heating power control system is based on duty modulation at a fixed operating frequency. An IHC with a rated power of 1000 W was implemented to verify the proposed online load estimation method by using both ferromagnetic and non-ferromagnetic cookware at different EHCRs; the estimation results were compared with measured results. The key contributions of this study are outlined as follows:

1. The study presents an online R_{eq} and L_{eq} estimation method for cookware. The proposed method requires only information about the resonant current i_r, namely the current at the high-side IGBT turn-off transient, the time in the first negative half-cycle, and the peak current during the natural resonant period in an HBSRC. To verify the proposed load estimation method, a measurement method based on the resonant voltage v_r and current i_r, representing fundamental frequency components, was also used to calculate R_{eq} and L_{eq}. The maximum error between the estimated R_{est} and measured R_{eq} for ferromagnetic cookware in normal situations was only 3.55%; thus, the proposed method can effectively and accurately control heating power. Moreover, the maximum errors between the estimated and measured resistance and inductance for cookware in abnormal situations were 7.14% and 2.78%, respectively. Thus, the method can effectively detect when no cookware is present on the heating coil or if non-ferromagnetic cookware is used and can turn off the heating power.

2. The proposed power control system is based on fundamental power $P_1(= \frac{1}{2}I_{rp1}^2 R_{est})$, which can be calculated using R_{est} and the amplitude of the resonant current I_{rp1}. Measurements revealed that the control system had a step response time of only 2 ms from no load to 1000 W and had accurate control in the steady state.

3. The experimental results for power control in emulated user operation reveal that the proposed method and control system in the IHC system can effectively estimate R_{eq} and L_{eq} online to detect cookware situations and determine whether to turn off or vary the heating power.

Author Contributions: Conceptualization, M.-S.H., Z.-F.L., C.-W.L. and Y.-M.M.; methodology, Z.-F.L.; software, J.-C.H., Y.-L.L. and Z.-F.L.; validation, Z.-F.L., J.-C.H. and Y.-L.L.; formal analysis, Z.-F.L., J.-C.H. and Y.-L.L.; investigation, Y.-M.M., C.-W.L. and Z.-F.L.; resources, M.-S.H., C.-W.L. and Y.-M.M.; data curation, Z.-F.L., J.-C.H. and Y.-L.L.; writing—original draft preparation, Z.-F.L.; writing—review and editing, M.-S.H.; visualization, Z.-F.L.; supervision, M.-S.H., C.-W.L. and Y.-M.M.; project administration, M.-S.H., C.-W.L. and Y.-M.M.; funding acquisition, M.-S.H. All authors have read and agreed to the published version of the manuscript.

Institutional Review Board Statement: Not applicable.

Informed Consent Statement: Not applicable.

Data Availability Statement: Not applicable.

Conflicts of Interest: The authors declare no conflict of interest.

References

1. Huang, M.S.; Liao, C.C.; Li, Z.F.; Shih, Z.R.; Hsueh, H.W. Quantitative Design and Implementation of an Induction Cooker for a Copper Pan. *IEEE Access* **2021**, *9*, 5105–5118. [CrossRef]
2. Lucía, O.; Maussion, P.; Dede, E.J.; Burdío, J.M. Induction Heating Technology and Its Applications: Past Developments, Current Technology, and Future Challenges. *IEEE Trans. Ind. Electron.* **2014**, *61*, 2509–2520. [CrossRef]
3. Cooktop Comparison: Gas, Electric and Induction. Available online: https://www.bijlibachao.com/appliances/cooktop-comparison-gas-electric-and-induction.html (accessed on 22 April 2016).
4. Residential Cooktop Performance and Energy Comparison Study. Available online: https://cao-94612.s3.amazonaws.com/documents/Induction-Range-Final-Report-July-2019.pdf (accessed on 30 July 2019).
5. Acero, J.; Burdio, J.M.; Barragan, L.A.; Navarro, D.; Alonso, R.; Garcia, J.R.; Monterde, F.; Hernandez, P.; Llorente, S.; Garde, I. The domestic induction heating appliance: An overview of recent research. In Proceedings of the 2008 Twenty-Third Annual IEEE Applied Power Electronics Conference and Exposition (APEC), Austin, TX, USA, 24–28 February 2008; pp. 651–657.
6. Sanz-Serrano, F.; Sagues, C.; Llorente, S. Power distribution in coupled multiple-coil inductors for induction heating appliances. In Proceedings of the 2015 IEEE Industry Applications Society Annual Meeting (IAS), Addison, TX, USA, 18–22 October 2015; pp. 1–8.
7. Kurose, H.; Miyagi, D.; Takahashi, N.; Uchida, N.; Kawanaka, K. 3-D Eddy Current Analysis of Induction Heating Apparatus Considering Heat Emission, Heat Conduction, and Temperature Dependence of Magnetic Characteristics. *IEEE Trans. Magn.* **2009**, *45*, 1847–1850. [CrossRef]
8. Namadmalan, A.; Moghani, J.S. Tunable Self-Oscillating Switching Technique for Current Source Induction Heating Systems. *IEEE Trans. Ind. Electron.* **2014**, *61*, 2556–2563. [CrossRef]
9. Chudnovsky, V.; Axelrod, B.; Shenkman, A.L. An approximate analysis of a starting process of a current source parallel inverter with a high-Q induction heating load. *IEEE Trans. Power Electron.* **1997**, *12*, 294–301. [CrossRef]
10. Vishnuram, P.; Ramachandiran, G.; Sudhakar Babu, T.; Nastasi, B. Induction Heating in Domestic Cooking and Industrial Melting Applications: A Systematic Review on Modelling, Converter Topologies and Control Schemes. *Energies* **2021**, *14*, 6634. [CrossRef]
11. Park, S.M.; Jang, E.; Joo, D.; Lee, B.K. Power Curve-Fitting Control Method with Temperature Compensation and Fast-Response for All-Metal Domestic Induction Heating Systems. *Energies* **2019**, *12*, 2915. [CrossRef]
12. Lian, G.; Hagel, R.; Unbehauen, R. A new approach to the nonlinear eddy current field coupled to the nonlinear heat transfer. *IEEE Trans. Ind. Appl.* **1995**, *31*, 733–736. [CrossRef]
13. Serrano, J.; Acero, J.; Lope, I.; Carretero, C.; Burdio, J.M.; Alonso, R. Modeling of domestic induction heating systems with non-linear saturable loads. In Proceedings of the 2017 IEEE Applied Power Electronics Conference and Exposition (APEC), Tampa, FL, USA, 26–30 March 2017; pp. 3127–3133.

14. Li, Z.; Chen, Q.; Zhang, S.; Ren, X.; Zhang, Z. A Mutual-Inductance-Based Impedance Model of Induction Cooker for Efficiency Improvement. In Proceedings of the 2019 22nd International Conference on Electrical Machines and Systems (ICEMS), Harbin, China, 11–14 August 2019; pp. 1–5.

15. Imai, T.; Sakiyama, K.; Hirota, I.; Omori, H. A study of impedance analysis for an induction heating device by applying a new interpolation method. *IEEE Trans. Magn.* **1997**, *33*, 2143–2146. [CrossRef]

16. Acero, J.; Carretero, C.; Lucía, Ó.; Alonso, R.; Burdio, J.M. Mutual Impedance of Small Ring-Type Coils for Multiwinding Induction Heating Appliances. *IEEE Trans. Power Electron.* **2013**, *28*, 1025–1035. [CrossRef]

17. Acero, J.; Alonso, R.; Burdio, J.M.; Barragan, L.A.; Puyal, D. Analytical equivalent impedance for a planar circular induction heating system. *IEEE Trans. Magn.* **2005**, *42*, 84–86. [CrossRef]

18. Jiménez, Ó.; Lucía, Ó.; Barragán, L.A.; Navarro, D.; Artigas, J.I.; Urriza, I. FPGA-Based Test-Bench for Resonant Inverter Load Characterization. *IEEE Trans. Ind. Inf.* **2013**, *9*, 1645–1654. [CrossRef]

19. Sarnago, H.; Lucía, O.; Burdio, J.M. A Versatile Resonant Tank Identification Methodology for Induction Heating Systems. *IEEE Trans. Power Electron.* **2018**, *33*, 1897–1901. [CrossRef]

20. Öztürk, M.; Oktay, U.; Yılmaz, N.; Yardibi, H.S.; Sinirlioğlu, S. Comparison of Pan Detection Methods for Single Switch Topology Used in Domestic Induction Cooking. In Proceedings of the 2020 International Conference on Smart Energy Systems and Technologies (SEST), Istanbul, Turkey, 7–9 September 2020; pp. 1–6.

21. Züngör, F.; Emre, B.; Öz, B.; Öztürk, M. A New Load Detection Method and Circuit Analysis for Quasi Resonant Inverter. In Proceedings of the 2021 10th International Conference on Renewable Energy Research and Application (ICRERA), Istanbul, Turkey, 26–29 September 2021; pp. 40–46.

22. Bono-Nuez, A.; Bernal-Ruíz, C.; Martín-del-Brío, B.; Pérez-Cebolla, F.J.; Martínez-Iturbe, A. Recipient size estimation for induction heating home appliances based on artificial neural networks. *Neural Comput. Appl.* **2017**, *28*, 3197–3207. [CrossRef]

23. Oh, Y.; Yeon, J.; Kang, J.; Galkin, I.; Oh, W.; Cho, K. Sensorless Control of Voltage Peaks in Class-E Single-Ended Resonant Inverter for Induction Heating Rice Cooker. *Energies* **2021**, *14*, 4545. [CrossRef]

24. Jiménez, Ó.; Lucía, Ó.; Urriza, I.; Barragán, L.A.; Navarro, D. Analysis and Implementation of FPGA-Based Online Parametric Identification Algorithms for Resonant Power Converters. *IEEE Trans. Ind. Inf.* **2014**, *10*, 1144–1153. [CrossRef]

25. Jiménez, O.; Barragán, L.A.; Navarro, D.; Artigas, J.I.; Urriza, I.; Lucía, O. FPGA-based harmonic computation through 1-bit data stream signals from delta-sigma modulators applied to induction heating appliances. In Proceeding of the 2011 Twenty-Sixth Annual IEEE Applied Power Electronics Conference and Exposition (APEC), Fort Worth, TX, USA, 6–11 March 2011; pp. 1776–1781.

26. Dominguez, A.; Otin, A.; Urriza, I.; Barragan, L.A.; Navarro, D.; Artigas, J.I. Load identification of domestic induction heating based on particle swarm optimization. In Proceeding of the IEEE 15th Workshop Control Modeling Power Electron. (COMPEL), Santander, Spain, 22–25 June 2014; pp. 1–6.

27. Sarnago, H.; Lucía, Ó.; Burdío, J.M. FPGA-Based Resonant Load Identification Technique for Flexible Induction Heating Appliances. *IEEE Trans. Ind. Electron.* **2018**, *65*, 9421–9428. [CrossRef]

28. Lucia, O.; Navarro, D.; Guillén, P.; Sarnago, H.; Lucia, S. Deep Learning-Based Magnetic Coupling Detection for Advanced Induction Heating Appliances. *IEEE Access* **2019**, *7*, 181668–181677. [CrossRef]

29. Villa, J.; Barragán, L.A.; Artigas, J.I.; Navarro, D.; Domínguez, A.; Cabeza, T. SoC-Based In-Cycle Load Identification of Induction Heating Appliances. *IEEE Trans. Ind. Electron.* **2021**, *68*, 6762–6772. [CrossRef]

30. Villa, J.; Navarro, D.; Dominguez, A.; Artigas, J.I.; Barragan, L.A. Vessel Recognition in Induction Heating Appliances—A Deep-Learning Approach. *IEEE Access* **2021**, *9*, 16053–16061. [CrossRef]

31. Domingo, N.; Barragán, L.A.; Montiel, J.M.M.; Domínguez, A.; Artigas, J.I. Fast power-frequency function estimation for induction heating appliances. *Electron. Lett.* **2017**, *53*, 498–500. [CrossRef]

32. Puyal, D.; Bernal, C.; Burdio, J.M.; Acero, J.; Millan, I. Methods and procedures for accurate induction heating load measurement and characterization. In Proceeding of the 2007 IEEE International Symposium on Industrial Electronics, Vigo, Spain, 4–7 June 2007; pp. 805–810.

33. Sarnago, H.; Lucía, Ó.; Mediano, A.; Burdío, J.M. Analytical Model of the Half-Bridge Series Resonant Inverter for Improved Power Conversion Efficiency and Performance. *IEEE Trans. Power Electron.* **2015**, *30*, 4128–4143. [CrossRef]

34. Yeon, J.; Cho, K.; Kim, H. A 3.6kW single-ended resonant inverter for induction heating applications. In Proceeding of the 2015 17th European Conference on Power Electronics and Applications (EPE'15 ECCE-Europe), Geneva, Switzerland, 8–10 September 2015; pp. 1–7.

35. Lai, Y.S.; Yu, M.H. Online Autotuning Technique of Switching Frequency for Resonant Converter Considering Resonant Components Tolerance and Variation. *IEEE J. Emerg. Sel. Top. Power Electron.* **2018**, *6*, 2315–2324. [CrossRef]